RSC Advances

PAPER

View Article Online
View Journal | View Issue

Cite this: *RSC Adv.*, 2022, **12**, 9130

Theoretical study of a derivative of chlorophosphine with aliphatic and aromatic Grignard reagents: $S_N2@P$ or the novel $S_N2@Cl$ followed by $S_N2@C$?†

Nandini Savoo,[a] Lydia Rhyman*[ab] and Ponnadurai Ramasami *[ab]

Received 13th January 2022
Accepted 15th March 2022

DOI: 10.1039/d2ra00258b

rsc.li/rsc-advances

The proposed S_N2 reactions of a hindered organophosphorus reactant with aliphatic and aromatic nucleophiles [Ye *et al.*, *Org. Lett.*, 2017, **19**, 5384–5387] were studied theoretically in order to explain the observed stereochemistry of the products. Our computations (using B3LYP as the functional) indicate that the reaction with the aliphatic nucleophile occurs through a backside $S_N2@P$ pathway while the reaction with the aromatic nucleophile proceeds through a novel $S_N2@Cl$ mechanism, followed by a frontside $S_N2@C$ mechanism.

Introduction

Organophosphorus derivatives possess significant value in disciplines such as asymmetric metal catalysis,[1] pest control,[2] medicine[3] and bioorganic chemistry.[4] An insight into their synthetic routes is thus essential.[1,5–8] One of the reactions often encountered in the synthesis of organophosphorus derivatives is the bimolecular nucleophilic substitution (S_N2) reaction at the trivalent tricoordinate phosphorus atom.[5,8–10] The S_N2 reaction at a trivalent phosphorus atom ($S_N2@P$) refers to the replacement of a substituent (leaving group, L) around the phosphorus atom by an electron-rich molecule (nucleophile, Nu^-). An $S_N2@P$ reaction occurs *via* the inversion and retention pathways in which molecular configuration around the phosphorus atom is inverted (P-inverted) and retained (P-retained), respectively [Fig. 1(a)].[10] The inversion pathway takes place by the attack of the Nu^- opposite to L which is synonymous to a backside S_N2 pathway ($S_N2@P$-b). Nucleophilic attack can also occur opposite to the lone pair of electrons on the phosphorus atom and on the same side as L in the retention pathway; this is analogous to a frontside S_N2 attack ($S_N2@P$-f).[10]

In the inversion and retention pathways of an archetypal $S_N2@P$ reaction, the initial interaction of the organophosphorus and the Nu^- reactants (R) generates a reactant complex (**RC**) which forms a pentacoordinate transition state (TS). The TS dissociates to form the product complex (**PC**) and finally the separate products (P). The R, **RC**, TS, **PC** and P make up the typical double-well potential energy surface (PES) [Fig. 1(b)].[11] An example is the retention pathway of the $PH_2Cl + Cl^-$ reaction which occurs through a double-well PES with a Berry pseudorotation about the phosphorus atom.[12] Studies also reported atypical PESs for $S_N2@P$ reactions when the bulkiness of the substituents around the phosphorus atom is changed.[11,13–15] An example is the nucleophilic attack at unhindered trivalent phosphorus atom centres which may result in a single-well PES [Fig. 1(c)] with a relatively stable pentacoordinate intermediate, which is known as the transition complex (TC).[12–15] The TC is in accordance with experimental reports.[16–19] Such a reaction is spontaneous; the reactants form a stable TC followed by the products without the formation of the **RC** or **PC**. An increase in the bulkiness of substituents around the trivalent phosphorus atom separates the TC from the R and P by the pre-TS and the post-TS, respectively. This results in a triple-well PES [Fig. 1(d)] which constitutes a stepwise Walden inversion with favourable energy barriers in an addition-elimination fashion.[6,10,11,14,20,21]

The bulkiness of substituents around the phosphorus atom is one of several factors governing the stereochemical consequences of $S_N2@P$ synthesis of organophosphorus derivatives. Other factors include the effect of neighbouring groups,[6,8] solvent[6,22] and the choice of nucleophile.[9,23–25] Ye *et al.* carried out an experimental study and they highlight the choice of nucleophile as a factor influencing the stereoselectivity of $S_N2@P$ reactions of organophosphorus compounds.[25] The study deals with the synthesis of tertiary phosphines from diastereomeric mixtures of secondary phosphine oxides in tetrahydrofuran (THF) in the presence of boron trihydride (BH_3) [Fig. 2(a)].[25] One of the steps in the synthesis [highlighted in blue in Fig. 2(a)] involves the replacement of a Cl atom bonded

[a]*Computational Chemistry Group, Department of Chemistry, Faculty of Science, University of Mauritius, Réduit 80837, Mauritius. E-mail: p.ramasami@uom.ac.mu*

[b]*Centre for Natural Product Research, Department of Chemical Sciences, University of Johannesburg, Doornfontein Campus, Johannesburg 2028, South Africa. E-mail: lyd.rhyman@gmail.com*

† Electronic supplementary information (ESI) available. See DOI: 10.1039/d2ra00258b

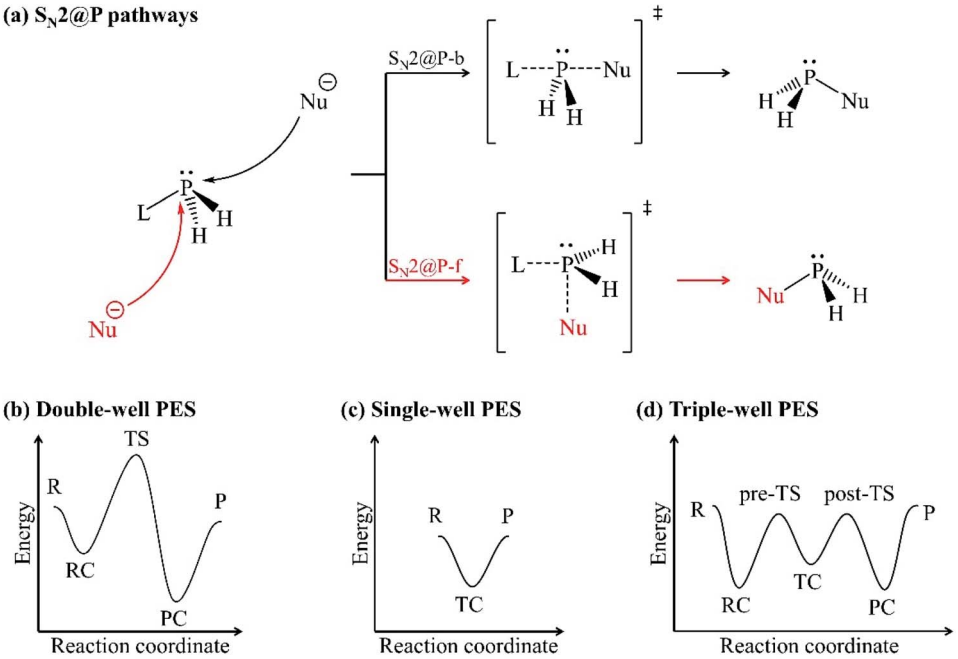

Fig. 1 (a) Inversion (S$_N$2@P-b, black) and retention (S$_N$2@P-f, red) pathways; (b) double-well; (c) single-well and; (d) triple-well PESs.

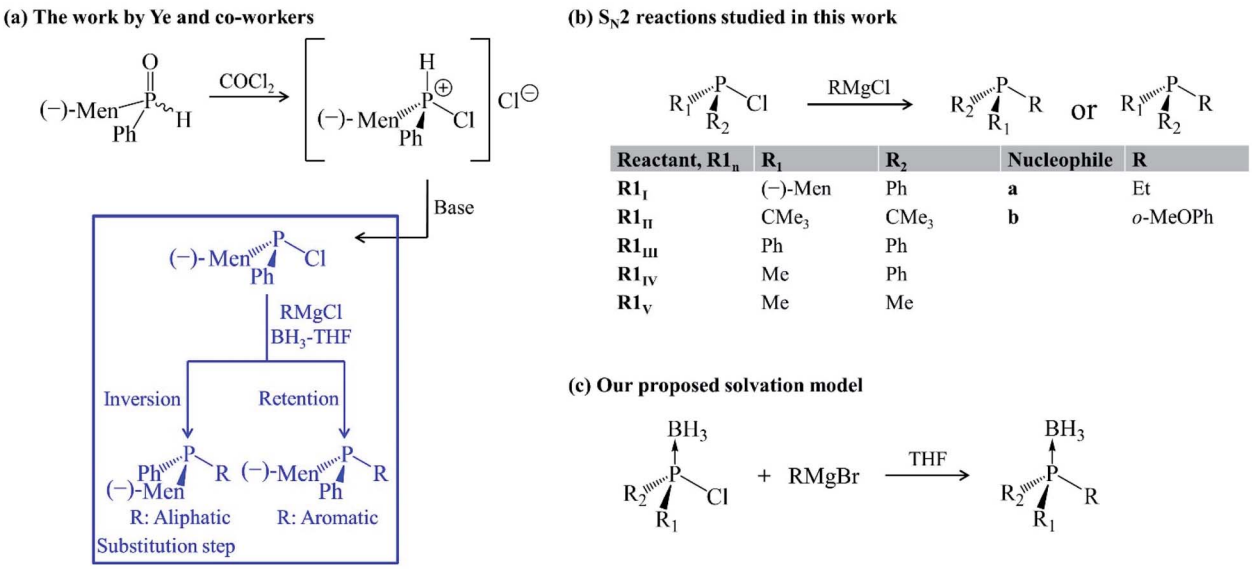

Reactant, R1$_n$	R$_1$	R$_2$	Nucleophile	R
R1$_I$	(−)-Men	Ph	a	Et
R1$_{II}$	CMe$_3$	CMe$_3$	b	*o*-MeOPh
R1$_{III}$	Ph	Ph		
R1$_{IV}$	Me	Ph		
R1$_V$	Me	Me		

Fig. 2 (a) Ye and co-workers' work.[25] The substitution step highlighted in blue shows the stereoselectivity of the reaction. (b) Gas-phase S$_N$2 reactions studied in this work. (c) Solvation model employed.

to the trivalent tertiary phosphorus atom by an R group from a Grignard reagent. The authors reported diastereomeric ratios (dr) of 98 : 2 and 1 : 99 for the P-inverted and P-retained organophosphorus products in the reactions involving an aliphatic and aromatic Grignard reagent, respectively.[25] Based on these observations, Ye *et al.* proposed that the aliphatic Grignard reagent attacks opposite to the leaving group Cl (S$_N$2@P-b) and the aromatic Grignard reagent attacks opposite to the lone pair of electrons on the phosphorus atom (S$_N$2@P-f).[25]

In continuation to our research programme to understand substitution reactions and our reports on the influence of ion-pair nucleophiles on S$_N$2 reactions,[26–28] we attempted a computational study of the reaction mechanisms which were proposed by Ye and co-workers.[25] The presence of BH_3 was considered when investigating the reactions in THF so as to mimic the solvation conditions in the experiment,[25] as it is reported that solvent systems constitute a crucial factor in influencing the stereoselectivity of reactions.[29] The occurrence of activation

barriers was explained using the distortion/interaction–activation strain model (D/I–ASM) of chemical reactivity.[30,31] The mechanisms that we determined do not only explain the experimental outcome[25] but also constitute a novel synthetic route, *via* S_N2@Cl mechanism, for organophosphorus derivatives which experimentalists may explore in cases where a control over stereoselectivity is required. Such an S_N2@Cl mechanism was reported by Zhang *et al.*[32] In addition, we investigated the steric effect on S_N2 reactions with Grignard reagents (**a** and **b**) as ion-pair nucleophiles in the gas phase and in THF. The results are shown in the ESI document in Fig. S1 and S2.†

Results and discussion

Mechanistic explanation of diastereoselectivity

In this section, we report on the mechanism by which the $\mathbf{R1_I}$ + **a** and $\mathbf{R1_I}$ + **b** reactions occur in order to explain their diastereoselectivity.[25] Depending on the orientation of the nucleophiles, we located several S_N2@P-b and S_N2@P-f pathways in the gas phase and in THF (see ESI†). Only those with the lowest Gibbs free activation barriers are reported in the manuscript (Fig. 3 and 4).

Both the gas-phase S_N2@P-b and S_N2@P-f pathways occur through a TS in which the Mg^{2+} cation interacts with both the Cl and C atoms and this causes the Cl–P–C bond angle to bend (Fig. 3). The bent Cl–P–C bond angle of the S_N2@P-b pathways is contrary to the typical near-linear TSs which are reported for anionic S_N2-b reactions.[14,33] This reflects the effect of the presence of the countercation Mg^{2+}. The small relative Gibbs free energy barriers ($\Delta\Delta G^{\neq}$) between the TSs of S_N2@P-b and S_N2@P-f pathways do not explain the drs (98 : 2 and 1 : 99 for the P-inverted and P-retained organophosphorus products, respectively) obtained in the experiment.[25] This mismatch between experiment and computations prompted us to consider the solvent effect.

We studied the solvent effect by incorporating a BH_3 molecule in the $\mathbf{R1_I}$ reactant and performing bulk solvation with THF as the solvent. Under such conditions, the S_N2@P-b pathways feature TSs with near-linear Cl–P–C bond angles. The PESs adopt a unimodal or a hill-and-well shape, which differs from anionic reactions.[14,15,29] The $\Delta\Delta G^{\neq}$ of 2.6 kcal mol^{-1} of the $\mathbf{R1_I}$ + **a** reaction (Fig. 4) indicates that the S_N2@P-b pathway is preferred. Indeed, the P-inverted organophosphorus stereoisomer was obtained in a higher dr (98 : 2).[25] Hence, the aliphatic nucleophile **a** prefers to react *via* the inversion pathway, as proposed by Ye *et al.*[25]

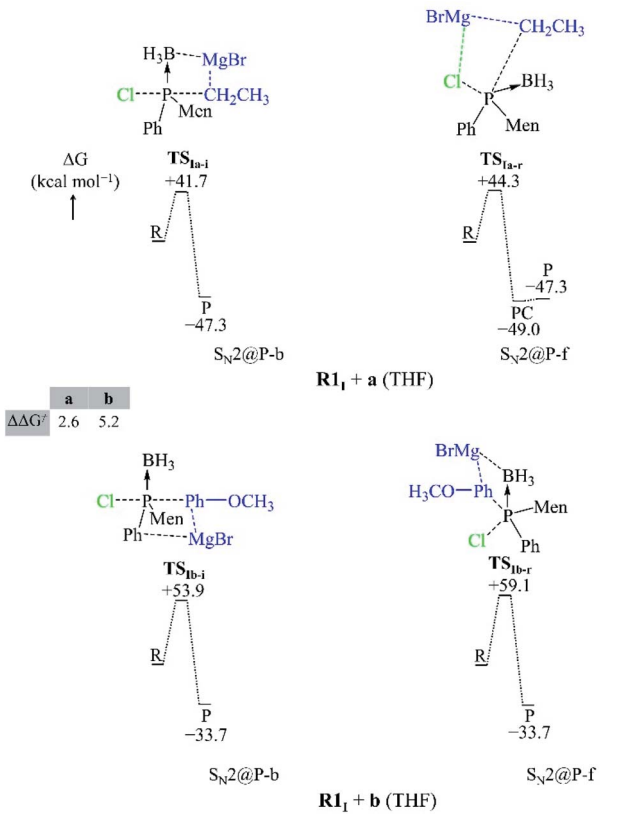

Fig. 3 Geometries of the TSs and PESs of the $\mathbf{R1_I}$ + **a** and $\mathbf{R1_I}$ + **b** S_N2@P reactions in the gas phase. The bond lengths/distances are in Å. The ΔG and $\Delta\Delta G^{\neq}$ are in kcal mol^{-1}.

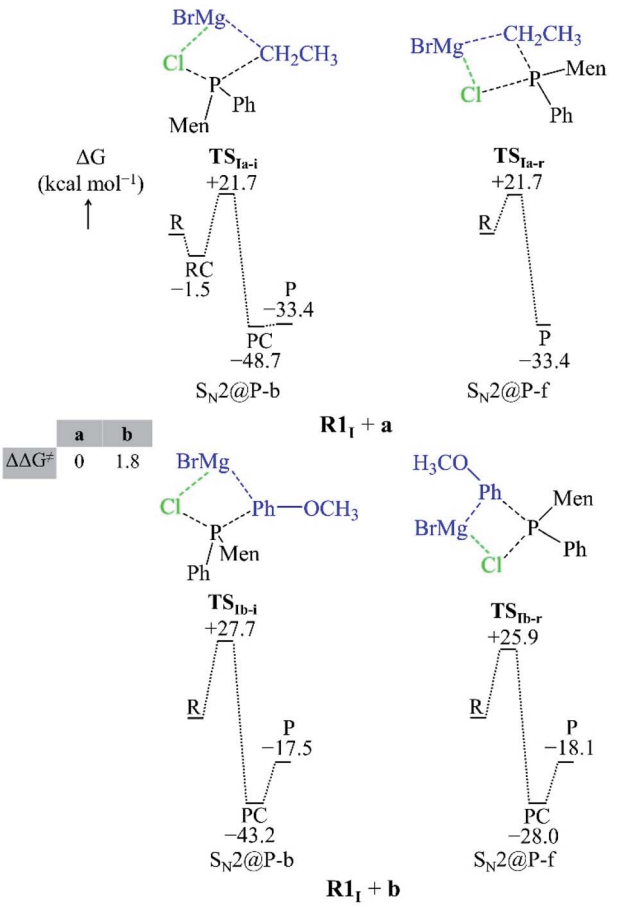

Fig. 4 Geometries of the TSs and PESs of the $\mathbf{R1_I}$ + **a** and $\mathbf{R1_I}$ + **b** S_N2@P reactions in THF. The bond lengths/distances are in Å. The ΔG and $\Delta\Delta G^{\neq}$ are in kcal mol^{-1}.

The $\Delta\Delta G^{\neq}$ (5.2 kcal mol^{-1}) of the $\mathbf{R1_I}$ + **b** reaction in THF shows that, similar to the $\mathbf{R1_I}$ + **a** reaction, the P-inverted stereoisomer should be obtained. However, the dr, higher for the P-retained stereoisomer (1 : 99),[25] shows that the S_N2@P-b mechanism is not at play. Hence, to explain the observations of Ye *et al.*,[25] we went back to the basics of charge distribution in a molecule. We therefore employed ESP maps to determine the possible modes of attack, or approach, of the nucleophile **b**. Owing to the coulombic nature of molecular interactions, ESP maps serve as good indicators of molecular regions which favour particular interactions; for instance, Bhasi *et al.* expanded the use of ESP maps to the successful location of TSs for atmospheric reactions which were previously thought to be barrierless.[34]

The ESP map of the organophosphorus reactant $\mathbf{R1_I}$ [Fig. 5(a)] shows a σ-hole at the extremity of and a belt of negative potential on the Cl atom. Previous reports related the σ-hole to the anisotropic charge distribution of the Cl atom in the molecule and to the occurrence of halogen-bonded complexes.[35–37] In this study, the σ-hole gives rise to a halogen-bonded **RC** [**RC** in Fig. 5(c)] with an electronic interaction energy of −1.9 kcal mol^{-1}; this qualifies as a halogen bonding interaction (that is, interaction between a halogen and a base) based on the study by Metrangolo *et al.*[38] Hence, we investigated the possibility of a reaction mechanism which is initiated by a halogen-bonded **RC**.

The C atom and the Mg^{2+} cation of nucleophile **b** interacts with the σ-hole and the belt of negative potential on the Cl atom, respectively, which forms **RC**. This halogen-bonded **RC** gives rise to a new type of S_N2 reaction, namely, an S_N2@Cl reaction. The **RC** [Fig. 5(c)] proceeds through a TS (**TS1**) where the C atom of the nucleophile **b** forms a bond with the Cl atom of $\mathbf{R1_I}$ and simultaneously breaks the P–Cl bond of $\mathbf{R1_I}$. As such, in the S_N2@Cl pathway, the Cl atom is the reactive centre and the organophosphorus moiety becomes the leaving group. The **TS1** leads to an intermediate (**INT1**) in which the Mg^{2+} cation is attracted to the negatively-charged P atom of the organophosphorus moiety. The **INT1** reorganises to form **INT2** where the Mg^{2+} cation shifts to interact with the electron density of the BH_3 moiety. This change in geometry brings the negatively-charged P atom in **INT2** in a position where an attack on the C atom of the *o*-MeOPhCl moiety is possible. This attack occurs through a frontside S_N2@C (S_N2@C-f) pathway. The **INT2** overcomes **TS2** [Fig. 5(c)] leading to the **PC** and finally to the separate products. This mechanism causes no umbrella flip around the P atom of the organophosphorus reactant and thus, the organophosphorus product retains its geometry around the P atom.

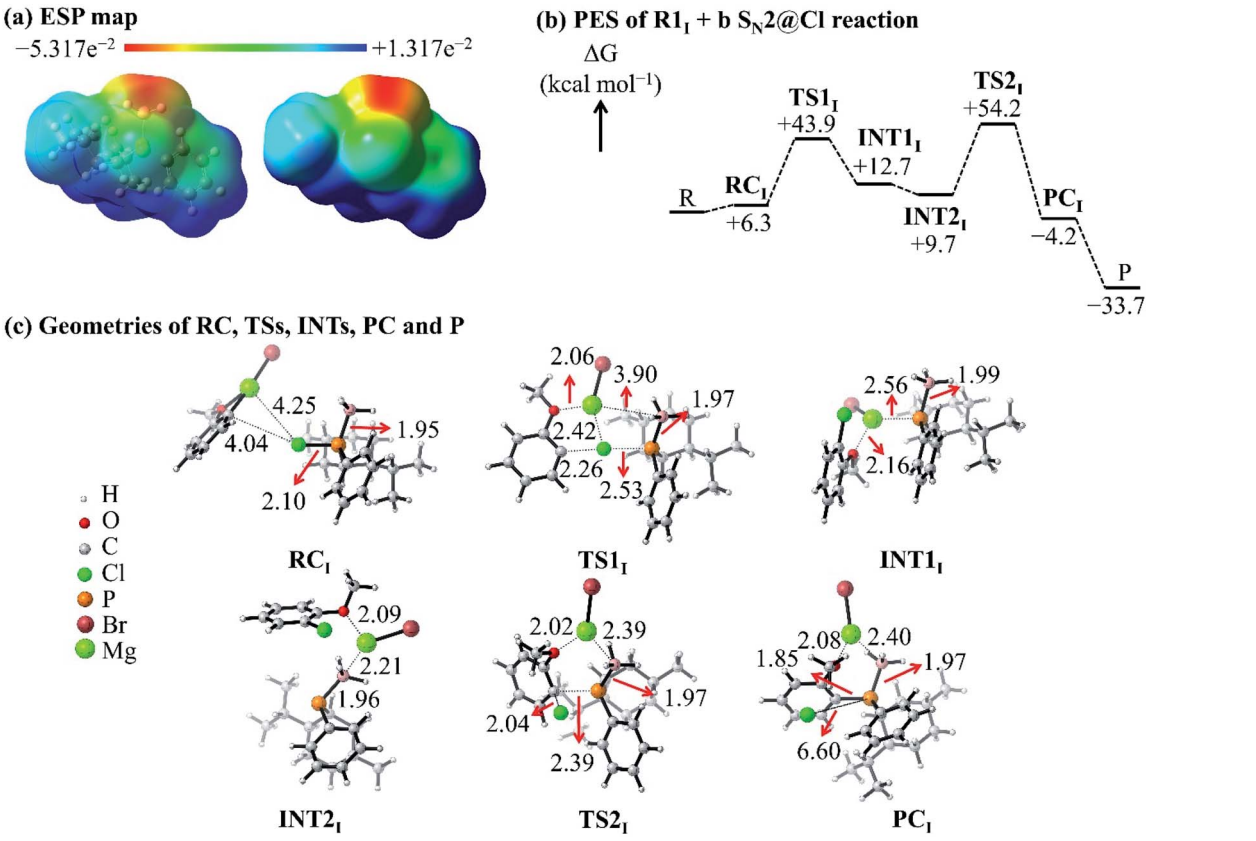

Fig. 5 (a) ESP map of the $\mathbf{R1_I}$ reactant. (b) PES of the $\mathbf{R1_I}$ + **b** S_N2@Cl reaction in THF. (c) Geometries of the RC, TSs, INTs, PC and P of the $\mathbf{R1_I}$ + **b** S_N2@Cl reaction in THF.

The ΔG of **TS1** [+43.9 kcal mol^{-1}, Fig. 5(b)] is lower than the Gibbs free activation energy of the inversion pathway of the S_N2@P reaction (+53.9 kcal mol^{-1}) by 10 kcal mol^{-1}. Hence, this explains the 1 : 99 dr obtained by Ye *et al.* for the P-retained product.[25] We thus confirmed that the reaction with nucleophile **b** occurs *via* an S_N2@Cl mechanism followed by an S_N2@C-f mechanism.

In order to investigate the solvation, strain and interaction factors behind the trend in reactivity of the **R1$_I$** + **a** and **R1$_I$** + **b** reactions, we employed the D/I–ASM. An analysis of the ASDs in Fig. 6 shows that the S_N2@P-b pathways are more stabilised by bulk solvation by THF than the S_N2@P-f pathways. This happens because of the change in geometries along the PESs; the reactants along the S_N2@P-b pathways deform to generate TSs with near-linear Cl–P–C bond angles (169.4° in **TS$_{Ia-i}$** and 175.3° in **TS$_{Ib-i}$**), whereas along the S_N2@P-f pathway, the reactants deform and lead to a TS with bent Cl–P–C bond angles (61.7° in **TS$_{Ia-r}$** and 72.0° in **TS$_{Ib-r}$**). There is more charge separation along the pathways which form the TSs with linear Cl–P–C bond angles than along pathways which lead to cyclic geometries.[26–28] The $\Delta E_{solvation}$ curve for the S_N2@Cl reaction indicates that the PES is most stabilised by THF at the start of the reaction (C–Cl–P bond angle is 174.7°). As the **INT1** is formed, the drop in charge separation causes less stabilisation by THF.

The **R1$_I$** + **a** reaction experiences more strain in the S_N2@P-b pathway which we ascribe to the umbrella flip about the phosphorus atom and to more geometrical deformation to reach the linear **TS$_{Ia-i}$** in THF. However, the S_N2@P-b pathway has a lower Gibbs free energy barrier than the S_N2@P-f pathway due to more favourable interaction between the deformed reactants and due to more stabilisation by THF. The initial stages of both the S_N2@P pathways of the **R1$_I$** + **b** reaction have similar strain curves while the S_N2@Cl reaction experiences higher strain. However, as **TS1** forms, the ΔE_{strain} lowers slightly [shown in magnified section in Fig. 5(b)] and the $\Delta E_{interaction}$ between the deformed reactants becomes comparable to the S_N2@P pathways. As the reaction progresses, the ΔE_{strain} stays lower than the S_N2@P-f pathway and comparable to the S_N2@P-b pathway, and eventually becomes the highest due to the extent of deformation of the reactant fragments involved in reaching the **INT1$_I$**. The interplay between the stabilisation by THF and reduction in strain while the TS forms that causes the S_N2@Cl mechanism to be the most preferred. Hence, we confirmed that (i) the **R1$_I$** + **a** reaction yields the P-inverted product in higher dr through an S_N2@P-b pathway and (ii) the **R1$_I$** + **b** reaction prefers the halogen bond-assisted S_N2@Cl pathway over the

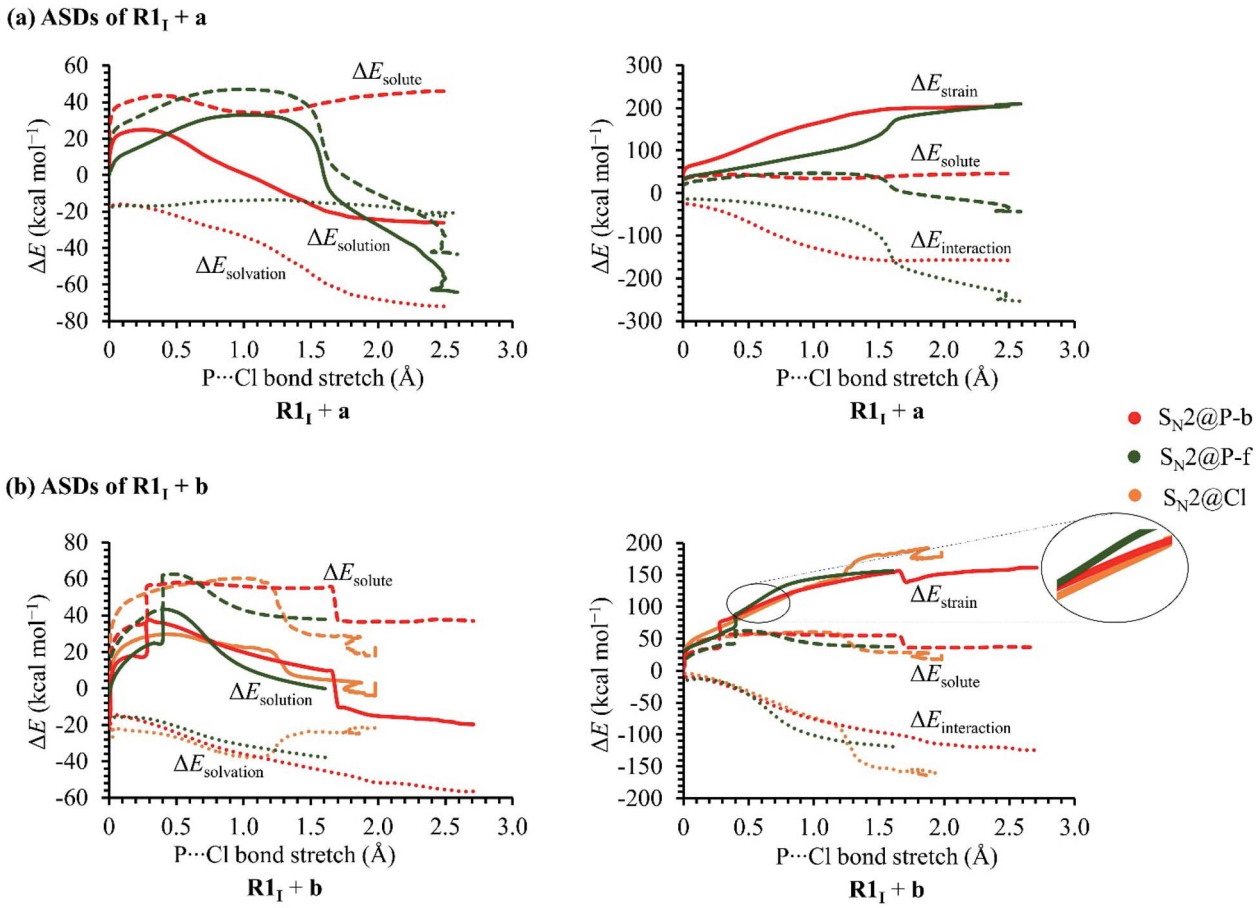

Fig. 6 ASDs of the (a) R1$_I$ + **a** and (b) R1$_I$ + **b** S_N2 reactions in THF.

Table 1 ΔG values, in kcal mol^{-1}, of the RCs, TSs, PCs and Ps of the S_N2@P-b and S_N2@P-f pathways of the $\mathbf{R1_I}$ + **a** and $\mathbf{R1_I}$ + **b** reactions in THF, computed using the M06-2X-D3/6-31++G(d,p) method. The values for the S_N2@P-f pathways are in parentheses

	$\mathbf{R1_I}$ + **a**	$\mathbf{R1_I}$ + **b**
RC	+1.9 (+1.9)	−2.7 (−1.7)
TS	+29.3 (+41.6)	+31.5 (+47.6)
PC	−48.7 (−59.0)	−2.9 (−7.6)
P	−50.3 (−50.3)	−34.3 (−37.2)

Table 2 ΔG values, in kcal mol^{-1}, of the **RC**, TSs, INTs, **PC** and P of the S_N2@Cl and S_N2@C-f pathways of the $\mathbf{R1_I}$ + **b** reaction in THF

S_N2@Cl pathway	
RC	+2.1
TS1	+42.2
INT1	+13.6
S_N2@C-f pathway	
INT2	+8.5
TS2	+34.4
PC	−21.2
P	−38.4

S_N2@P-b pathway by a factor of 10 kcal mol^{-1}. The reactions were also investigated using the M06-2X-D3/6-31++G(d,p) method. The ΔG values are listed in Tables 1 and 2 in kcal mol^{-1}.

A comparison of the energy values shows that the $\mathbf{R1_I}$ + **a** reaction has a lower activation barrier of +29.3 kcal mol^{-1} in the S_N2@P-b pathway and thus, the reaction occurs through the S_N2@P-b pathway. This explains the formation of the products of inverse geometry in the experiment.[25] The $\mathbf{R1_I}$ + **b** reaction has activation barriers of +31.5, +47.6 and +42.2 kcal mol^{-1} in the S_N2@P-b, S_N2@P-f and S_N2@Cl pathways, respectively. Hence, the $\mathbf{R1_I}$ + **b** reaction also prefers the S_N2@P-b pathway. This differs from the results obtained using the B3LYP functional and does not explain the formation of the products of retained geometry in the experiment.[25]

The TSs were optimised using the MP2 method to obtain more accurate energy values. Due to the large size of the organophosphorus reactant and due to the computationally-demanding nature of the MP2 method, the ΔG values were computed only for the TSs instead of along the whole PESs. We employed the 6-31G(d) basis set because using any higher basis set causes the TS to converge to the **RC**. Table 3 shows the ΔG of the TSs of the S_N2@P-b, S_N2@P-f, S_N2@Cl and S_N2@C-f pathways. It was observed that the TS of the S_N2@P-b pathway has the lowest activation energy. Hence, the S_N2@P-b pathway is preferred, similar to the M06-2X-D3 results. This is in contrast to the B3LYP results. It was thus deduced that the product of retained geometry may be obtained through a different reaction mechanism instead of those investigated in this manuscript.

Table 3 ΔG, in kcal mol^{-1}, of the TSs of the S_N2@P-b, S_N2@P-f, S_N2@Cl and S_N2@C-f pathways

	S_N2@P-b	S_N2@P-f	S_N2@Cl	S_N2@C-f
TS	+32.4	+48.1	+37.2	+42.6

Conclusions

Ye *et al.* substituted the chlorine atom in a derivative of chlorophosphine and obtained the P-inverted and P-retained organophosphorus products on using aliphatic and aromatic Grignard reagents, respectively.[25] In this manuscript, we determined the reaction mechanisms of these two reactions ($\mathbf{R1_I}$ + **a** and $\mathbf{R1_I}$ + **b**) using the B3LYP/6-31++G(d,p) method. We also highlighted the use of a model of the THF-solvated reaction system with a dative bond between the P and B atoms to account for the presence of the BH_3 molecule. The lower Gibbs free activation barrier of the S_N2@P-b pathway of the $\mathbf{R1_I}$ + **a** reaction explains the formation of the P-inverted product in THF. Our D/I–ASM analyses attribute the preference of the S_N2@P-b pathway to more favourable interaction between the deformed reactants and more stabilisation by THF. In the case of the $\mathbf{R1_I}$ + **b** reaction, the S_N2@P mechanism fails to explain the formation of the P-retained product. In fact, our computations point to a halogen bond-assisted S_N2@Cl mechanism. The S_N2@Cl mechanism occurs with a lower free Gibbs activation barrier than the S_N2@P pathways and is followed by an S_N2@C-f mechanism. The preference of the S_N2@Cl mechanism resulted from greater stabilisation by THF and reduction in strain while the $\mathbf{TS1_I}$ forms.

We also investigated the effect of decreasing steric crowding of the phosphorus atom of the $\mathbf{R1_n}$ organophosphorus reactants. The results are reported in the ESI.† As the bulkiness of the substituents decreases, the $\mathbf{R1_n}$ + **a** reactions occur through the S_N2@P-b pathways; the decrease in bulkiness lowers the Gibbs free energy barriers of the S_N2@P-b pathways on account of more stabilisation by THF and lower deformational strain in the initial stages of the reactions. As the bulkiness of the substituents decreases in the $\mathbf{R1_n}$ + **b** reactions, the relative Gibbs free energy barrier of the S_N2@P-b pathways becomes lower than that of the S_N2@Cl pathway due to the interplay between the strain and interaction components. Hence, a consideration of competing interactions, such as halogen bonding, becomes significant when determining the course of an S_N2 reaction, especially in the presence of bulky substituents which hinder the reactive centre.

When the reactions were repeated using the M06-2X-D3/6-31++G(d,p) and MP2/6-31G(d) methods, the preference of the reaction changed to the S_N2@P-b pathway. This does not explain the formation of the retention products in the experiment and shows that the computational findings depend on the level of theory used for computations. It is known that different methods give different results due to the different level of approximations.[39–42] This may lead to benchmark studies with respect to such organophosphorus reactions.

Methodology

Full optimisation with no symmetry constraints was performed using the B3LYP[43–45] hybrid functional and the 6-31++G(d,p) basis set in the gas phase. We selected this method based on previous reports involving S_N2@P.[20,33,46–48] The stationary points were characterised by frequency computations to verify that the TSs have only one imaginary frequency[49] and these were checked by intrinsic reaction coordinate (IRC) computations.

The same computational method was employed based on the polarisable continuum model (PCM)[50] to perform bulk solvation with THF by incorporating BH_3 in the reaction system to mimic the experiment conditions.[25] This procedure is reported in the literature.[6] All the computations were carried out at 298.15 K and 1 atm. The reactions are reported in terms of the ΔG with respect to the separate reactants, unless otherwise specified.

We performed a non-covalent interaction (NCI) analysis of selected TSs using the Multiwfn program.[51–53] The NCI plots, which are shown in the ESI in Fig. S3,† allow for a visualisation of non-covalent interactions between molecular fragments as real-space surfaces. Within the NCI framework, the sign of λ_2 enables identification of the interaction type. Attractive interactions are negative, van der Waals interactions occur close to zero and steric repulsions are positive. The Visual Molecular Dynamics program was used to visualise the molecules in 3D.[54] The Gnuplot 4.2 program[55] and Ghostscript interpreter[56] were employed to generate the 2D plots.

Moreover, the D/I–ASM of chemical reactivity was employed to explain the trends in reactivity along the reaction.[30,31,57,58] In the D/I–ASM, the energy along the reaction coordinate is decomposed into its strain and interaction energies. Eqn (1) shows how the D/I–ASM relates the relative electronic energy of a reaction (ΔE) to the relative strain (ΔE_{strain}) and relative interaction (ΔE_{int}) energies of the deformed reactant fragments along the reaction coordinate (ζ).

$$\Delta E(\zeta) = \Delta E_{\text{strain}}(\zeta) + \Delta E_{\text{int}}(\zeta) \quad (1)$$

The $\Delta E_{\text{strain}}(\zeta)$ corresponds to the relative electronic energy necessary to distort the reactant fragments throughout the reaction while the $\Delta E_{\text{int}}(\zeta)$ corresponds to the interactions between the deforming reactant fragments.

The D/I–ASM was also applied in THF to investigate the effect of solvation ($\Delta E_{\text{solvation}}$). The solvent-phase PES is described in terms of its components, solute energy and solvation energy, as in eqn (2). The solvation energy englobes the solute–solvent interaction, as well as the formation of the solvent cavity.

$$\Delta E_{\text{solution}}(\zeta) = \Delta E_{\text{solute}}(\zeta) + \Delta E_{\text{solvation}}(\zeta) \quad (2)$$

We obtained the $\Delta E_{\text{solute}}(\zeta)$ from the SP energy values of the reactant fragments in gas phase, computed using their geometry from solvent-phase computations. Eqn (3) shows a further breakdown of the ΔE_{solute} into ΔE_{strain} and ΔE_{int}.

$$\Delta E_{\text{solute}}(\zeta) = \Delta E_{\text{strain}}(\zeta) + \Delta E_{\text{int}}(\zeta) \quad (3)$$

The reaction coordinate was considered as the IRC projected onto P⋯Cl bond stretch, which constitutes the activation strain diagram (ASD).

In another attempt to explain the outcome of the experiment computationally under the experiment conditions employed by Ye *et al.*,[25] the effect of a temperature of 193.15 K was considered on the ΔG; the results are reported in the ESI.† ΔE at both at 298.15 K and 193.15 K are reported in the ESI.† The ExcelAutomat tool[59–61] facilitated file manipulation and file extraction. GaussView 6,[62] Chemcraft[63] and CylView[64] were employed to visualise structures. All computations were carried out in Gaussian 09 [65] and Gaussian 16 [66] suites using the SEAGrid computing facilities.[67–71] Explicit details about the computational methods are found in the ESI.†

According to several reports, the use of dispersion correction is necessary for the investigation of non-covalent interactions between the nucleophile and the σ-hole of the chlorine atom.[29,72–74] Hence, these reactions were studied using the M06-2X functional and dispersion correction was considered; full optimisation computations were performed using the dispersion-corrected M06-2X-D3.[72,75–78] Moreover, the second-order Møller–Plesset (MP2)[79–83] method was also employed in order to obtain more reliable energy values. The energy values were compared with the results obtained using the B3LYP/6-31++G(d,p) method.

Author contributions

PR was responsible for project administration, conceptualisation, supervision and writing – review & editing.

LR was responsible for conceptualisation, supervision and writing – review & editing.

NS was responsible for conceptualisation, investigation, data curation and writing – original draft.

Conflicts of interest

There are no conflicts to declare.

Acknowledgements

The authors are grateful to the Higher Education Commission (HEC) of Mauritius. The authors are also grateful to SEAGrid and South African CHPC for providing computing facilities.

References

1 K. Shioji, A. Tashiro, S. Shibata and K. Okuma, *Tetrahedron Lett.*, 2003, **44**, 1103.
2 M. Etō, *Organophosphorus Pesticides: Organic and Biological Chemistry*, CRC Press, Inc., Boca Raton, 1979.
3 Y. Song, J. J. Vittal, N. Srinivasan, S.-H. Chan and P.-H. Leung, *Tetrahedron: Asymmetry*, 1999, **10**, 1433.
4 K. M. Pietrusiewicz and M. Zablocka, *Chem. Rev.*, 1994, **94**, 1375.
5 O. I. Kolodiazhnyi, *Tetrahedron: Asymmetry*, 2012, **23**, 1.

6 H. Zijlstra, T. León, A. de Cózar, C. F. Guerra, D. Byrom, A. Riera, X. Verdaguer and F. M. Bickelhaupt, *J. Am. Chem. Soc.*, 2013, **135**, 4483.
7 G.-Q. Lin, Q.-D. You and J.-F. Cheng, *Chiral Drugs: Chemistry and Biological Action*, John Wiley & Sons, Inc., New Jersey, 2011.
8 O. I. Kolodiazhnyi, *Asymmetric Synthesis in Organophosphorus Chemistry*, Wiley-VCH, Germany, 2017.
9 J.-L. Montchamp, *Topics in Current Chemistry: Phosphorus Chemistry I*, Springer International Publishing, Switzerland, 2015.
10 O. I. Kolodiazhnyi and A. Kolodiazhna, *Tetrahedron: Asymmetry*, 2017, **28**, 1651.
11 M. A. van Bochove, M. Swart and F. M. Bickelhaupt, *Phys. Chem. Chem. Phys.*, 2009, **11**, 259.
12 Y. Ding, J. Mu and L. Gong, *J. Chin. Chem. Soc.*, 2013, **60**, 327.
13 M. A. van Bochove and F. M. Bickelhaupt, *Eur. J. Org. Chem.*, 2008, **2008**, 649.
14 M. A. van Bochove, M. Swart and F. M. Bickelhaupt, *J. Am. Chem. Soc.*, 2006, **128**, 10738.
15 M. A. van Bochove, M. Swart and F. M. Bickelhaupt, *ChemPhysChem*, 2007, **8**, 2452.
16 I. Granoth and J. C. Martin, *J. Am. Chem. Soc.*, 1978, **100**, 7434.
17 K. B. Dillon and T. C. Waddington, *J. Chem. Soc., Chem. Commun.*, 1969, 1317a.
18 W. S. Sheldrick, A. Schmidpeter, F. Zwaschka, K. B. Dillon, A. W. G. Platt and T. C. Waddington, *J. Chem. Soc., Dalton Trans.*, 1981, 413.
19 A. P. Marchenko, G. N. Koidan, A. N. Hurieva, A. B. Rozhenko and A. N. Kostyuk, *Heteroat. Chem.*, 2016, **27**, 12.
20 O. Dmitrenko, C. Thorpe and R. D. Bach, *J. Org. Chem.*, 2007, **72**, 8298.
21 O. I. Kolodiazhnyi and A. O. Kolodiazhna, *Phosphorus, Sulfur Silicon Relat. Elem.*, 2017, **192**, 621.
22 O. I. Kolodiazhnyi, *Pure Appl. Chem.*, 2019, **91**, 43.
23 O. I. Kolodiazhnyi, S. Sheiko and E. V. Grishkun, *Heteroat. Chem.*, 2000, **11**, 138.
24 M. Oliana, F. King, P. N. Horton, M. B. Hursthouse and K. K. Hii, *J. Org. Chem.*, 2006, **71**, 2472.
25 J.-J. Ye, S.-Z. Nie, J.-P. Wang, J.-H. Wen, Y. Zhang, M.-R. Qiu and C.-Q. Zhao, *Org. Lett.*, 2017, **19**, 5384.
26 J. Z. A. Laloo, L. Rhyman, P. Ramasami, F. M. Bickelhaupt and A. de Cózar, *Chem.–Eur. J.*, 2016, **22**, 4431.
27 J. Z. A. Laloo, L. Rhyman, O. Larrañaga, P. Ramasami, F. M. Bickelhaupt and A. de Cózar, *Chem.–Asian J.*, 2018, **13**, 1138.
28 N. Savoo, J. Z. A. Laloo, L. Rhyman, P. Ramasami, F. M. Bickelhaupt and J. Poater, *J. Comput. Chem.*, 2020, **41**, 317.
29 S. Jain and K. Vanka, *J. Am. Chem. Soc.*, 2020, **124**, 8019.
30 W.-J. van Zeist and F. M. Bickelhaupt, *Org. Biomol. Chem.*, 2010, **8**, 3118.
31 P. Vermeeren, S. C. C. van der Lubbe, C. F. Guerra, F. M. Bickelhaupt and T. A. Hamlin, *Nat. Protoc.*, 2020, **15**, 649.
32 X. Zhang, J. Ren, S. M. Tan, D. Tan, R. Lee and C.-H. Tan, *Science*, 2019, **363**, 400.
33 P. Farahani, M. Lundberg and H. O. Karlsson, *Chem. Phys.*, 2013, **425**, 134.
34 P. Bhasi, Z. P. Nhlabatsi and S. Sitha, *Phys. Chem. Chem. Phys.*, 2016, **18**, 13002.
35 T. Clark, M. Hennemann, J. S. Murray and P. Politzer, *J. Mol. Model.*, 2007, **13**, 291.
36 P. Politzer, J. S. Murray and T. Clark, *Phys. Chem. Chem. Phys.*, 2010, **12**, 7748.
37 P. Politzer, J. S. Murray and T. Clark, *Phys. Chem. Chem. Phys.*, 2013, **15**, 11178.
38 P. Metrangolo, H. Neukirch, T. Pilati and G. Resnati, *Acc. Chem. Res.*, 2005, **38**, 386.
39 M. Linder and T. Brinck, *Phys. Chem. Chem. Phys.*, 2013, **15**, 5108.
40 X. Xu and W. A. Goddard, *Proc. Natl. Acad. Sci. U. S. A.*, 2004, **101**, 2673.
41 G. S. J. Armstrong, M. A. Khokhlova, M. Labeye, A. S. Maxwell, E. Pisanty and M. Ruberti, *Eur. Phys. J. D*, 2021, **75**, 209.
42 M. D. Hack, R. G. A. R. Maclagan, G. E. Scuseria and M. S. Gordon, *J. Chem. Phys.*, 1996, **104**, 6628.
43 A. D. Becke, *Phys. Rev. A*, 1988, **38**, 3098.
44 C. Lee, W. Yang and R. G. Parr, *Phys. Rev. B: Condens. Matter Mater. Phys.*, 1988, **37**, 785.
45 B. Miehlich, A. Savin, H. Stoll and H. Preuss, *Chem. Phys. Lett.*, 1989, **157**, 200.
46 C. Fish, M. Green, R. J. Kilby, J. M. Lynam, J. E. McGrady, D. A. Pantazis, C. A. Russell, A. C. Whitwood and C. E. Willans, *Angew. Chem., Int. Ed.*, 2006, **45**, 3628.
47 D. Mandal, B. Mondal and A. K. Das, *J. Phys. Chem. A*, 2012, **116**, 2536.
48 E. V. Jennings, K. Nikitin, Y. Ortin and D. G. Gilheany, *J. Am. Chem. Soc.*, 2014, **136**, 16217.
49 L. Fan, L. Versluis, T. Ziegler, E. J. Baerends and W. Ravenek, *Int. J. Quantum Chem.*, 1988, **34**, 173.
50 J. Tomasi, B. Mennucci and R. Cammi, *Chem. Rev.*, 2005, **105**, 2999.
51 T. Lu and F. Chen, *J. Comput. Chem.*, 2012, **33**, 580.
52 E. R. Johnson, S. Keinan, P. Mori-Sánchez, J. Contreras-García, A. J. Cohen and W. Yang, *J. Am. Chem. Soc.*, 2010, **132**, 6498.
53 A. Otero-de-la-Roza, E. R. Johnson and J. Contreras-García, *Phys. Chem. Chem. Phys.*, 2012, **14**, 12165.
54 W. Humphrey, A. Dalke and K. Schulten, *J. Mol. Graphics*, 1996, **14**, 33.
55 T. Williams and C. Kelley, *Gnuplot, Version 4.2: An interactive plotting program*, 2007, http://www.gnuplot.info/.
56 *Ghostscript, Version 9.53.3*, http://www.artifex.com.
57 I. Fernandez and F. M. Bickelhaupt, *Chem. Soc. Rev.*, 2014, **43**, 4953.
58 T. A. Hamlin, B. van Beek, L. P. Wolters and F. M. Bickelhaupt, *Chem.–Eur. J.*, 2018, **24**, 5927.
59 J. Z. A. Laloo, N. Laloo, L. Rhyman and P. Ramasami, *J. Comput.-Aided Mol. Des.*, 2017, **31**, 667.

60 J. Z. A. Laloo, N. Savoo, N. Laloo, L. Rhyman and P. Ramasami, *ExcelAutomat 1.2: Automation of natural bond order analysis and extraction of electronic energies from quantum chemical calculations*, Global Science & Technology Forum (GSTF), 2018, pp. 72–76.
61 J. Z. A. Laloo, N. Savoo, N. Laloo, L. Rhyman and P. Ramasami, *J. Comput. Chem.*, 2019, **40**, 619.
62 R. Dennington, T. A. Keith and J. M. Millam, *GaussView, Version 6*, 2016.
63 G. A. Zhurko and D. A. Zhurko, *ChemCraft, Version 1.7*, 2013. http://www.chemcraftprog.com.
64 C. Y. Legault, *CYLview 1.0b*, Université de Sherbrooke, 2009.
65 M. J. Frisch*et al.*, *Gaussian 09, Revision D.01*, Gaussian, Inc.Wallingford CT, 2009.
66 M. J. Frisch*et al.*, *Gaussian 16, Revision B.01*, Gaussian, Inc., Wallingford CT, 2016.
67 S. Pamidighantam, S. Nakandala, E. Abeysinghe, C. Wimalasena, S. R. Yodage, S. Marru and M. Pierce, *Procedia Comput. Sci.*, 2016, **80**, 1927.
68 N. Shen, Y. Fan and S. Pamidighantam, *J. Comput. Sci.*, 2014, **5**, 576.
69 R. Dooley, K. Milfeld, C. Guiang, S. Pamidighantam and G. Allen, *J. Grid Comput.*, 2006, **4**, 195.
70 K. Milfeld, C. Guiang, S. Pamidighantam and J. Giuliani, *Cluster Computing through an Application-oriented Computational Chemistry Grid. Proceedings of the 2005 Linux Clusters: The HPC Revolution*, 2005.
71 This work used the Extreme Science and Engineering Discovery Environment (XSEDE), which is supported by National Science Foundation grant number OCI-1053575.
72 L. Goerigk and S. Grimme, *Phys. Chem. Chem. Phys.*, 2011, **13**, 6670.
73 R. Sedlak, T. Janowskic, M. Pitoňákd, J. Řezáča, P. Pulayc and P. Hobza, *J. Chem. Theory Comput.*, 2013, **9**, 3364.
74 M. Breugst and J. J. Koenig, *Eur. J. Org. Chem.*, 2020, **2020**, 5473.
75 Y. Zhao and D. G. Truhlar, *Theor. Chem. Acc.*, 2008, **120**, 215.
76 L. Goerigk, A. Hansen, C. Bauer, S. Ehrlich, A. Najibi and S. Grimme, *Phys. Chem. Chem. Phys.*, 2017, **19**, 32184.
77 M. Walker, A. J. A. Harvey, A. Sen and C. E. H. Dessent, *J. Phys. Chem. A*, 2013, **117**, 12590.
78 I. Singh, A. A. El-Emam, S. K. Pathak, R. Srivastava, V. K. Shukla, O. Prasad and L. Sinha, *Mol. Simul.*, 2019, **45**, 1029.
79 M. J. Frisch, M. Head-Gordon and J. A. Pople, *Chem. Phys. Lett.*, 1990, **166**, 275.
80 M. J. Frisch, M. Head-Gordon and J. A. Pople, *Chem. Phys. Lett.*, 1990, **166**, 281.
81 M. Head-Gordon, J. A. Pople and M. J. Frisch, *Chem. Phys. Lett.*, 1988, **153**, 503.
82 S. Sæbø and J. Almlöf, *Chem. Phys. Lett.*, 1989, **154**, 83.
83 M. Head-Gordon and T. Head-Gordon, *Chem. Phys. Lett.*, 1994, **220**, 122.